

High-Contrast Laser Marking of Microelectronic Packaging Modules

N. Liu¹, Kh. Moumanis¹, D. Carrier¹, M. Bilodeau², V. Pomerleau², B. Foisy², J.J. Dubowski^{1*},

¹ Laboratory for Quantum Semiconductors and Photon-based BioNanotechnology, Interdisciplinary

Institute for Technological Innovation (3IT), Université de Sherbrooke, Québec J1K 2R1, Canada,

² Centre de Collaboration MiQro Innovation (C2MI), IBM Canada Ltd, Bromont, Quebec, J2L 1A3, Canada

*E-mail: jan.j.dubowski@usherbrooke.ca

Laser marking is an attractive technique allowing high-speed and high spatial resolution identification of materials, mechanical parts, tools or packaging modules for traceability, advertising, security or trademark protection reasons. The laser marking process, however, is very sensitive to the chemical composition, physical properties and texture of processed surfaces. We have investigated the role of surface chemistry and morphology of nickel-plated copper lids in achieving high optical contrast marking with a Q-switch Nd:YAG laser. Profilometry, scanning electron microscopy and x-ray photoelectron spectroscopy measurements have been carried out to characterize investigated samples. The results indicate that a low-contrast marking results from a poor ability of the laser to nanostructure the thermally unstable Ni(OH)₂-rich surface. The primary mechanism of high-quality marking is related to laser-induced smoothing of the surface and not to the modification of the chemical composition of the irradiated material. However, thermal processing of the lids in air or N₂ environments in the 300-350 °C range, before laser irradiation, has a pronounced effect on the chemical composition as well as on the color of the nickel-plated lids. Laser marking of such color-modified lids leads to drastically improved both resolution and contrast of the process.

DOI: 10.2961/jlmn.2015.02.0013

Keywords: Laser marking, Q-switch Nd:YAG laser, nickel plating, IC packaging, X-ray photoelectron spectroscopy, nickel oxide

1. Introduction

The marking of metal-based packaging modules designed for holding microelectronic circuits is an important step in the device fabrication processes and in providing valuable information both to the manufacturers and their clients. Conventional methods of marking, such as those based on ink-jet printing, suffer from the drawbacks related to the cost of consumables, durability of marking and flexibility of the process [1]. With the introduction of lasers in 1960s, many investigations have been carried out into the laser ability to mark engineering materials. Laser marking of microelectronic modules and packages is a technique used in the microelectronics industry to identify production lots and, e.g., manufacturing dates. The aim of the laser marking is to perform a permanent trace on the surface of the material in order to make it readable and recognizable. Laser marking has advanced systematically over recent 30 years, replacing inkjet marking in many cases due to its high speed and inherent flexibility [2]. In that context, marking of nickel plated packages of integrated circuits (IC) continues to grow and is clearly one of the most diverse market segments. Magnetic properties, corrosion resistance and solderability of nickel plating are properties that have contributed the most to this success [3]. Among various parameters affecting the appearance of laser marked surfaces, the uncontrollable surface morphology and chemistry modification of different substrates could be the source of a reduced contrast marking. The related stud-

ies have investigated laser parameters, such as laser beam scanning speed, line width, frequency and power [4]. Fewer works have focused on investigation of the influence of surface morphology and surface chemical composition on the quality of laser marking [5].

We have investigated a series of nickel-plated Cu lids of IC packaging modules with the goal to determine the origin of a variable quality of laser marking produced with a Q-switch Nd:YAG laser. The focus of our study was surface morphology and surface chemistry of the investigated lids before and after laser irradiation.

2. Experiments

A total of 24 Ni-plated (2.5-7.6 μm) Cu lids of IC packaging modules were investigated in this work. The laser marking of original lids was carried out with a Q-switch Nd:YAG laser (RSM 50D, Rofin-Sinar) operating at 26 A and a 7 kHz repetition rate. The marking was achieved by employing an f-theta lens system with X-Y computer controlled scanning at 200 mm/s. Thermally processed (annealed) lids were marked with a similar Q-switch laser (Qmark, Quantronix) operating between 21 and 28 A and at 1 to 21 kHz to maintain a fluence of 1 mJ/pulse [6]. The laser beam scanning speed was adjusted in the range of 400~1000 mm/s to maintain overlap of 25 μm between 200 μm diameters spots. The average brightness intensity (gray level) of the marked and unmarked regions was obtained from the analysis of microscopic images of the laser

marked samples. The optical contrast was calculated from the ratio of gray levels of marked and unmarked regions [4].

A stylus surface profilometer (Dektak 150, Veeco Instruments, Inc.) was used to measure surface roughness of the samples. The measurements were taken using a $2.5\text{ }\mu\text{m}$ radius stylus with a 3.0 mg contact force at $3.3\text{ }\mu\text{m/s}$ scan speed. Low-resolution 3D maps were obtained by scanning a length of $100\text{ }\mu\text{m}$ in X direction with a $4\text{ }\mu\text{m}$ stepping in Y direction. These 3D maps provided a clear picture of surface morphology of $100\text{ }\mu\text{m} \times 100\text{ }\mu\text{m}$ regions characterized by the root-mean-square (RMS) roughness, R_q . More detailed analysis of surface morphology was obtained by collecting scanning electron microscopy (SEM) images with a Supra 55 SEM microscope operating at 15 keV .

Surface chemistry has been investigated with the X-ray photoelectron spectroscopy (XPS) technique employing a Kratos Analytical, AXIS Ultra DLD spectrometer equipped with a $150\text{ W Al K}\alpha$ source and operating at a base pressure of 1×10^{-9} Torr. The surface survey and high resolution scans were observed in constant energy modes with 50 and 20 eV pass energy filters, respectively. The size of an analyzed area on the investigated samples was set at $220\text{ }\mu\text{m} \times 220\text{ }\mu\text{m}$. The XPS spectra were recorded for samples after laser irradiation and after annealing in a conventional furnace. The collected data were processed using Casa XPS 2.3.15 software. To compensate for the surface charging effect, all XPS data binding energies were referenced to the adventitious C (C_{adv}) 1s peak at the BE of 285.0 eV .

3. Results and Discussion

3.1 Laser marking contrast investigation

Fig. 1 shows microscopic image of sample No 2 with low contrast (a) and sample No 11 with high contrast (b) marking. It clearly shows a superior contrast between marked and unmarked regions on sample No 11. The laser marked region on sample No 2 is only weakly distinguishable from the initial (unmarked) region.

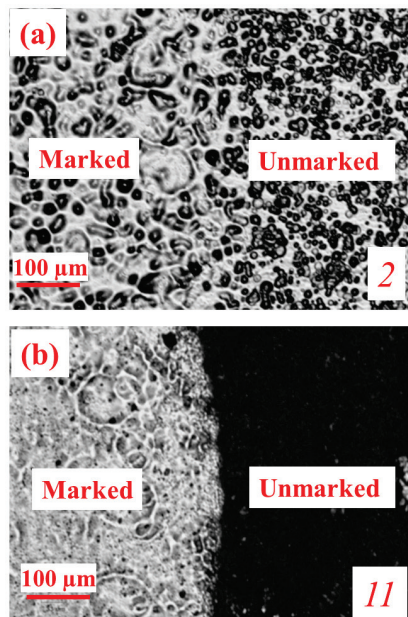


Fig. 1 Microscopic images of sample No 2 with low contrast (a) and sample No 11 with high contrast (b) laser marking.

Table 1 summarizes gray scale intensities (GSI) of 6 samples selected from the group of investigated samples (No. 11, 14, 18, 5, 17 and 2). It can be seen that sample No 11 exhibits the largest intensity ratio between the unmarked and laser marked regions, while sample No 2 shows the weakest laser marking contrast.

Table 1 Intensity of marked and unmarked regions of 6 samples selected from the pool of 24 samples.

Sample No	GSI		GSI ratio Mrk/Unk
	Marked	Unmarked	
11	172	58	2.97
14	207	71	2.92
18	157	110	1.43
5	196	142	1.38
17	122	96	1.27
2	144	115	1.25

3.2 Surface morphology investigation

In order to investigate the effects of surface morphology on the achievable laser marking contrast, we compare in Table 2 the R_q values for the samples discussed in Table 1. Sample No 11, which exhibits the largest marking contrast, also shows the lowest roughness of the laser marked region. At the same time, sample No 2, which exhibits the poorest marking contrast, shows the highest roughness of the laser marker region. Generally, it seems that the increasing ratio of R_q^{Mrk}/R_q^{Unk} is associated with the decreasing contrast of laser marking. The samples from the poor marking contrast group (No 18, 5, 17 and 2) are characterized by relatively high values of R_q^{Unk} . However, as discussed in Sec. 3.3, the samples from this group exhibit also an excessive concentration of Ni(OH)_2 that is drastically reduced following the irradiation with the laser. For such samples, laser induced surface morphology cannot be separated from a modification of its chemical composition. In contrast, the surface of chemically more stable and initially (chemically) nanostructured samples exhibit high marking contrast, as observed in Fig. 1b. The interaction of a laser with such samples (No 11 and 14) leads to smoothing of their surfaces that reflect white light with an increased efficiency.

Table 2 Root-mean-square (R_q) roughness of as-received (unmarked) and laser marked samples.

Sample No	R_q (nm)		R_q^{Mrk}/R_q^{Unk}
	Marked	Unmarked	
11	352	547	0.6
14	334	541	0.6
18	636	956	0.7
5	481	478	1.0
17	602	670	0.9
2	793	719	1.1

Fig. 2 shows SEM images of non-processed and laser marked surfaces of samples No 14, 5, and 17. Based on the contrast and surface morphology measurements in Table 1 and Table 2, the marking quality decreases from sample No 14 and 5 to 17. Note the differences in the surface mor-

phology of non-processed regions: the roughest initial surface characterizes the worst laser marking quality sample. On the processed regions of samples No 14 and 5, a series of laser fabricated spots can be seen quite clearly. The spots on the sample No 17, however, are almost invisible.

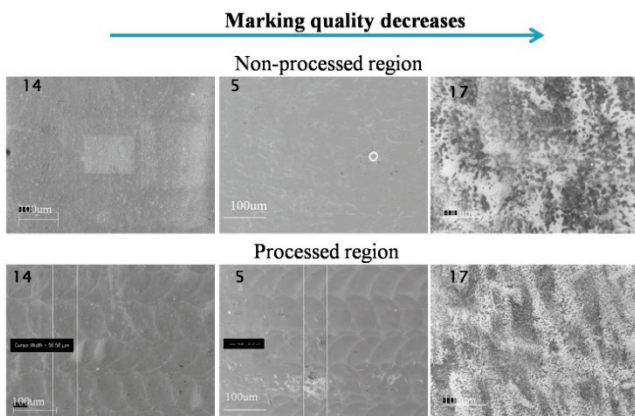


Fig. 2 SEM images of non-processed and processed regions of samples No 14, 5 and 17.

3.3 Surface chemical investigation

Fig. 3 shows the Ni 2p 3/2 XPS spectra of non-processed and processed regions of the sample No 14, which belongs to the group of samples exhibiting a good quality laser marking. The spectra are fitted with the asymmetric line shape and plasmon loss peaks for Ni metal (red) and an empirical fit of the NiO (green) and Ni(OH)₂ (blue) line shapes [7]. The offset of the higher binding energy end of the background was used to improve the fit of the peak shapes. This background offset is determined using an iterative approach while monitoring a residual plot of the 2p 3/2 area [8]. Peak positions of these chemical compounds are presented in Table 3.

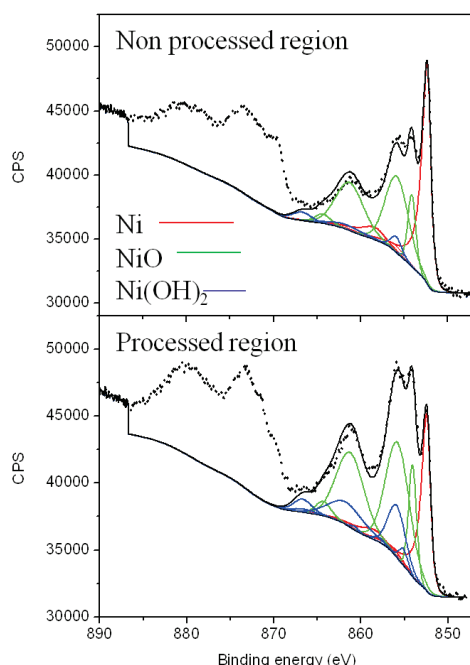


Fig. 3 Ni XPS spectra of non-processed and processed regions of sample 14. The XPS data envelope is shown with a dotted line (...) and the results of fitting are shown with a solid black line (—).

Table 3 Binding energy of chemical compounds used to fit the Ni 2p 3/2 spectrum.

	Peak 1 (eV)	Peak 2 (eV)	Peak 3 (eV)	Peak 4 (eV)	Peak 5 (eV)	Peak 6 (eV)
Ni	852.4	856.0	858.4			
NiO	854.1	855.8	861.2	864.3	866.7	
Ni(OH) ₂	855.1	855.9	857.9	860.7	861.7	866.7

The atomic percentage of Ni, NiO and Ni(OH)₂ for non-processed and processed regions of the sample No 14 is shown in Table 4. These results indicate the increasing concentration of NiO and Ni(OH)₂ on the laser processed sites.

Table 4 Atomic percentage of Ni, NiO and Ni(OH)₂ of non-processed and processed regions of the sample No 14.

	Ni	NiO	Ni(OH) ₂
Non-processed	25.52	54.80	19.68
Processed	18.96	58.24	22.81

In Table 5, we present atomic percentage of Ni, NiO and Ni(OH)₂ observed on non-processed regions of the samples No 14, 5, 9 and 17 that are listed in an order representing a decreasing laser marking quality. It can be seen that the increasing concentration of Ni(OH)₂ coincides with a decreased quality marking.

Table 5 Atomic percentage of Ni, NiO and Ni(OH)₂ on the as-received surface of selected samples. The intensity ratio was calculated based on gray scale of the as-received and laser marked material.

Sample	GSI ratio	Ni	NiO	Ni(OH) ₂
14	2.92	25.52	54.80	19.68
5	1.38	27.06	38.86	36.83
9	1.29	15.71	35.16	48.56
17	1.27	20.98	28.57	48.18

For comparison, the concentration of Ni, NiO and Ni(OH)₂ on the surface of laser irradiated samples No 14, 5, 9 and 17 are listed in Table 6. It can be seen that the chemical composition of all the samples are similar and no trend could be observed that would correspond to the decreasing/increasing contrast of laser marking.

Table 6 Atomic percentage of Ni, NiO and Ni(OH)₂ on the laser processed surface of selected samples.

Sample	GSI ratio	Ni	NiO	Ni(OH) ₂
14	2.92	18.96	58.24	22.81
5	1.38	18.56	66.15	15.41
9	1.29	18.86	57.15	23.26
17	1.27	15.14	66.90	15.94

Based on these results, we conclude that the high quality marking observed for the sample No 14 is not due to the differences in surface chemical composition between as received and laser processed surfaces. The laser smoothing of the surface appears in this case to be the main reason of the observed laser marking contrast. However, a drastic reduction of Ni(OH)₂ has been observed on the surface of

laser irradiated samples exhibiting poor quality marking (No 5, 9, 17). Surface roughness of such samples remained relatively unaffected by irradiation with the laser, as observed in Table 1 for the samples No 5 and 17, or even increased following the laser irradiation, as observed for sample No 2.

3.4 Thermal processing before laser marking

Since the excessive concentration of Ni(OH)_2 on the as-received surfaces of the investigated lids was found related to poor quality marking, we have also investigated laser marking of samples that were thermally processed to reduce Ni(OH)_2 known to decompose at temperatures exceeding 300°C [9]. Table 7 compares the XPS results obtained for samples before and after heating at 300 and 350°C in N_2 and air for 20 minutes. It shows that the annealing even at 300°C drastically reduces surface concentration of Ni(OH)_2 . At the same time, a 2.7-fold and 3-fold increase of NiO has been observed.

Table 7 Atomic percentage of Ni, NiO and Ni(OH)_2 on the surface of as-received and annealed samples at 300 and 350°C for 20 minutes in N_2 and air.

	Ni	NiO	Ni(OH)_2
Before heating	20.98	28.57	48.18
Heating at 300°C in N_2	0.24	76.31	23.44
Heating at 350°C in N_2	0.5	76.97	22.45
Heating at 300°C in air	0.24	83.84	15.93
Heating at 350°C in air	0.23	87.59	13.68

In addition to significant changes of the chemical composition, the samples annealed at 350°C exhibited significant transformation of their color. Fig. 4 shows optical image of a reference sample (before heating) and samples annealed in air at 300°C (Air 300deg) and 350°C (Air 350deg) and in N_2 at 300°C (Nitrogen 300deg) and 350°C (Nitrogen 350deg). It can be seen that the sample annealed in N_2 underwent their color change from silver to light blue (Nitrogen 300deg) and to deep blue (Nitrogen 350deg). In comparison, the samples annealed in air, underwent their color changed from silver to light yellow (Air 300deg) and deep yellow (Air 350deg). As illustrated in Fig. 4, laser marking of thermally processed samples, especially those annealed at 350°C , produced clearly visible marks with a contrast far exceeding that of any of the high-quality marks fabricated on as-received samples.

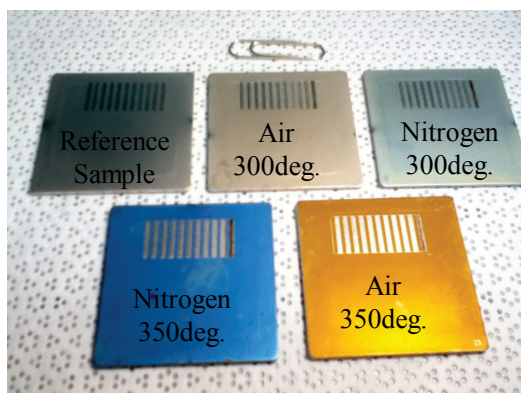


Fig. 4 Images of a reference sample and samples heated in air and N_2 at 300°C and 350°C .

Nickel oxide has been widely studied as an electrochromatic material undergoing color transformation during OH desorption induced by reactions involving ion injection and heating [10]. The oxide rich films have been reported to be fully colored while the reduced oxidation films are bleached or transparent [11]. We employed XPS measurements to investigate the origin of color transformation and study $\text{NiO}/\text{Ni(OH)}_2$ ratio in thermally treated material [12].

Fig. 5 shows the Ni 2p XPS spectra of the non-marked yellow (Air 350deg) and blue (Nitrogen 350deg) samples. It can be seen that, in comparison with Fig. 3, the quantity of metal Ni at 852.4 eV in the yellow material has diminished to near the background level. Furthermore, all five peaks of NiO (with binding energies listed in Table 3) show increased intensities while slightly reduced intensities of Ni(OH)_2 related peaks have also been observed.

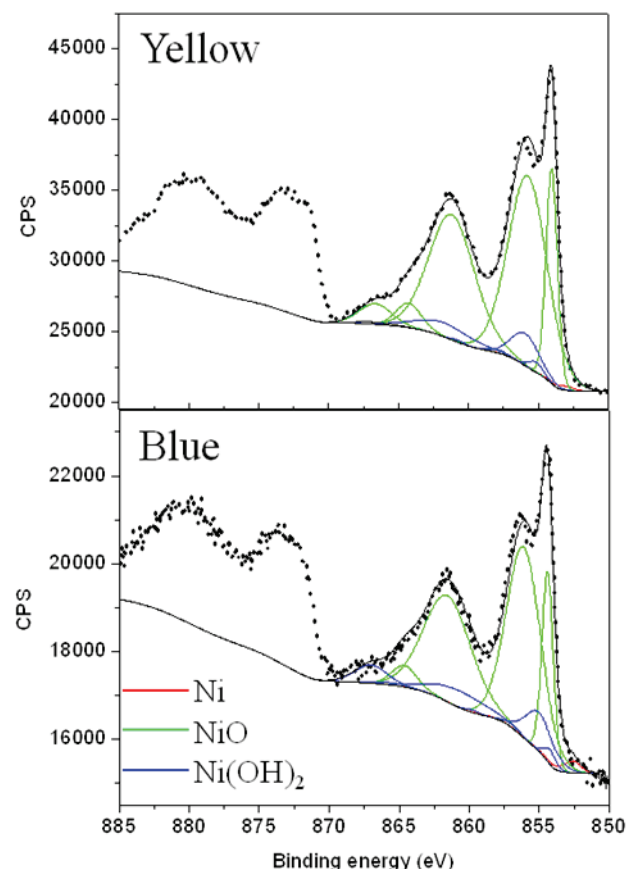


Fig. 5 Ni 2p XPS spectra of yellow and blue surfaces. The XPS envelope is shown with a dotted line (...) and the results of fitting are shown with a solid black line (—).

Fig. 6 shows the O 1s XPS spectra of non-marked region on the reference, yellow and blue samples surfaces. The dash-line peaks in the region of 530-536 eV originate from the oxygen bonded to C adsorbates on the surface [13, 14]. The NiO components include two major O peaks assigned at 529.8 and 531.3 eV. The first peak corresponds to O bonded to a regular Ni oxide crystal and the second peak corresponds to oxygen atoms in positions adjacent to Ni vacancies ($\text{NiO}(\text{def})$) within the oxide structure. The peak at 531.4 eV is assigned to hydroxide bonded to nickel: Ni(OH)^+ . The peak at 532.9 eV on the reference sample is

assigned to H₂O/O₂ remaining on the surface. The peak at 532.6 eV in the blue sample originates from the nitrate nickel oxides formed during heating in the N₂ environment. From Fig. 5 and 6, it is estimated that the ratio of NiO/Ni(OH)₂ is 6.4 and 3.42 on yellow and blue surface, respectively, which compares to 0.59 observed for the reference silver-like sample.

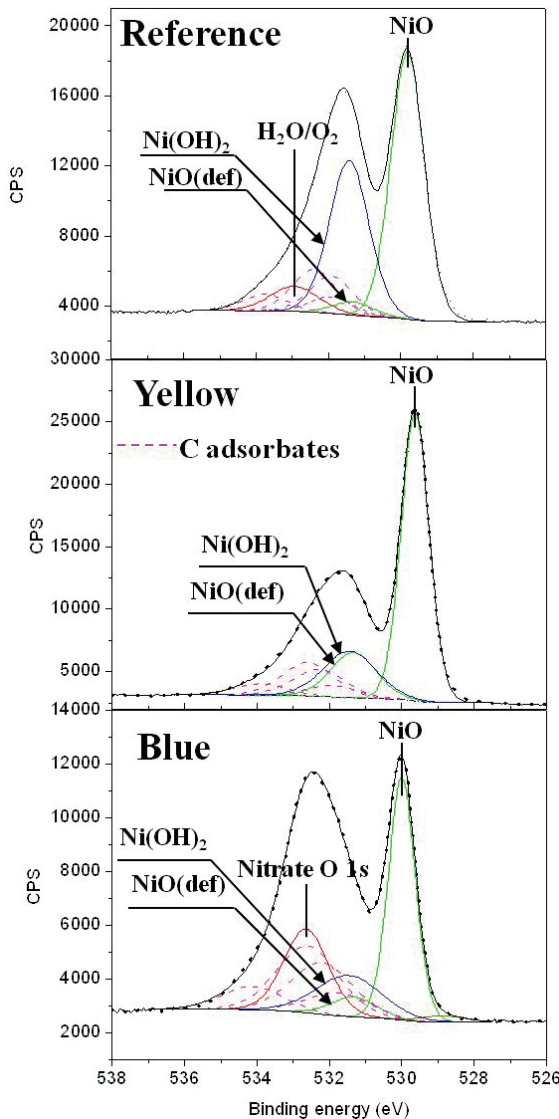


Fig. 6 O 1s XPS spectra of non-marked region of yellow and blue surfaces. The XPS data envelope is shown with a dotted line (...) and the results of fitting are shown with a solid black line (—).

It has been reported that normally transparent (bleached) thin films of Ni(OH)₂ undergo oxidation in an OH⁻ environment that results in formation of yellow to brown films absorbing light in the visible region of the spectrum [11]:



The nickel oxide/hydroxides mixture has been described by NiO(OH) with octahedral nickel-oxygen coordination [12]. The formation of pale blue NiO_x films has also been observed with an electrolytic process followed by chemical vapor deposition [12]. These experiments have revealed that the bleached state and film coloration depend on the

number of Ni(OH)₂ sites lacking in water molecules and extraction/insertion of protons and water molecules in the structure of these films.

In the marked region, the XPS ratios of NiO/Ni(OH)₂ were reduced from 6.4 to 2.81 and 3.42 to 2.72 on the yellow and blue substrates, respectively. In the marked region of the samples preheated at 300 °C, those ratios were reduced from 5.26 to 2.97 for the samples annealed in air, and from 3.26 to 2.92 for the samples annealed in N₂ (data not shown here). Thus the NiO/Ni(OH)₂ ratio in the marked region of annealed samples (2.72 – 2.97) and of the high-quality laser marked as-received sample No 14 (2.6) fall in the close range of chemical compositions. It is interesting to note that the laser irradiation of as-received and 300 °C annealed samples yields surfaces that, observed under a near normal incidence, reflect more efficiently white light than the non-irradiated surface. The opposite effect is observed under a grazing incidence angle, as illustrated in Fig. 4, which indicates laser-induced formation of a diffusively scattering surface. However, laser marking of the blue and yellow lids produced smooth surfaces that appear always brighter to the eye, regardless of the observation angle.

4. Conclusion

The results of this study have indicated that non-uniformly Ni-plated Cu lids of microelectronic packaging modules could result in a poor quality laser marking not correctable by varying laser parameters. Thermal annealing at 350°C of the as-fabricated lids produces their coloration. The annealing in air yields yellow material, while annealing in N₂ yields blue material. This color change is related to decomposition of Ni(OH)₂ and extraction/insertion of protons and water molecules in the structure of the films. Thermal processing of Ni-plated lids offers attractive conditions for high-contrast and high-resolution laser marking with the Q-switch Nd:YAG laser.

5. Acknowledgement

This work was supported by the Natural Science and Engineering Research Council of Canada Engage Grant No. EGP 437014 – 12, Discovery Grant No. 122795-2010 and the program of the Canada Research Chair in Quantum Semiconductors (JJD). The authors are indebted to Mr. David Danovitch for fruitful discussions. Technical assistance of the Université de Sherbrooke Centre de caractérisation de matériaux (CCM) in collecting XPS data and the Centre de recherche en nanofabrication et en nanocaractérisation (CRN²) is greatly appreciated.

6. References

- [1] Y. M. Noor, S. C. Tam, L. E. N. Lim and S. Jana: *J. Mater. Process. Technol.* 42, (1994) 95.
- [2] L. E. Gordon: US Patent 4,922,077, (1990)
- [3] J. Sudagar, J. Lian and W. Sha: *J. Alloys Compd.* 571, (2013) 183.
- [4] J. F. Ready, D. F. Farson and T. Feeley: "LIA handbook of laser materials processing: laser marking/branding" ed. by (Laser Institute of America Orlando 2001) p.715.
- [5] B. Dusser, Z. Sagan, H. Soder, N. Faure, J.-P. Colombier, M. Jourlin and E. Audouard: *Opt. Express* 18, (2010) 2913.

- [6] R. Stanowski, O. Voznyy and J. J. Dubowski: *JLMN* 1, (2006) 17.
- [7] M. C. Biesinger, B. P. Payne, A. P. Grosvenor, L. W. Lau, A. R. Gerson and R. S. C. Smart: *Appl. Surf. Sci.* 257, (2011) 2717.
- [8] M. C. Biesinger, B. P. Payne, L. W. Lau, A. Gerson and R. S. C. Smart: *Surf. Interface Anal.* 41, (2009) 324.
- [9] T. Sato, T. Nakamura and F. Ozawa: *J. Appl. Chem. Biotechnol.* 25, (1975) 583.
- [10] D. Wruck and M. Rubin: *J. Electrochemi. Soc.* 140, (1993) 1097.
- [11] M. K. Carpenter, R. S. Conell and D. A. Corrigan: *Sol. Energ. Mat.* 16, (1987) 333.
- [12] M. Chigane and M. Ishikawa: *J. Chem. Soc. Faraday Trans.* 94, (1998) 3665.
- [13] N. Liu and J. J. Dubowski: *Appl. Surf. Sci.* 270, (2013) 16.
- [14] B. P. Payne, M. C. Biesinger and N. S. McIntyre: *Electron. Spectrosc. Relat. Phenom.* 184, (2009) 29.

(Received: September 1, 2014, Accepted: March 3, 2015)